

# Microencapsulated Carbon Black Suspensions for Restoration of Electrical Conductivity

Sen Kang, Amanda R. Jones, Jeffrey S. Moore, Scott R. White, and Nancy R. Sottos\*

**Robust microcapsules are prepared with carbon black suspensions high in solids loading (up to 0.2 g/mL) for electrical conductivity restoration. Oxidized carbon black is rendered more hydrophobic through surface functionalization with octadecylamine by two different methods. Functionalization significantly improves dispersability and suspension stability of carbon black in hydrophobic solvents such as *o*-dichlorobenzene (*o*-DCB), enabling encapsulation by *in situ* emulsion polymerization. Upon crushing, microcapsules containing functionalized carbon black (FCB) suspensions exhibit significant particle release relative to microcapsules filled with unfunctionalized carbon black. Release of carbon black is further enhanced by the addition of two types of core thickeners, epoxy resin or poly 3-hexylthiophene (P3HT). Full conductivity restoration (100% restoration efficiency) of damaged silicon anodes is achieved by crushing microcapsules containing FCB suspensions with P3HT. Hydrophobic surface functionalization of carbon black and the addition of core thickeners are both critical for achieving stable microcapsules capable of significant particle release and efficient conductivity restoration.**

## 1. Introduction

Damage triggered release of microencapsulated conductive core materials has enabled autonomous restoration of electrical conductivity in a broken circuit.<sup>[1,2]</sup> Encapsulation of several different types of conductive core materials has been reported

in the literature.<sup>[2–8]</sup> Odom et al. observed the formation of conductive charge transfer salt on a broken circuit upon the release of two reactive liquid components from a dual capsule system.<sup>[4]</sup> Blaiszik et al. prepared conductive liquid metal (Ga-In alloy) filled microcapsules and demonstrated rapid recovery of conductivity in a mechanically damaged circuit.<sup>[1]</sup> Microcapsules containing carbon nanotube and graphene suspensions have also been reported to restore electrical conductivity upon particle release.<sup>[2,3]</sup> Another major avenue for conductivity restoration is through the intrinsic self-healing of dynamic conjugated polymers.<sup>[9,10]</sup>

In contrast to electric circuits, battery electrodes are composite materials consisting of active particles such as graphite or silicon and a polymer binder. Conductive carbon black nanoparticles are often added to the electrodes to fill the interstitial regions and increase electrical conductivity.<sup>[11]</sup> Silicon anodes undergo enormous volume expansion and contraction (ca. 400% volume change) upon lithium insertion and extraction. Continued cycling results in cracking or pulverization of the silicon, and ultimately, destruction of the conductive network.<sup>[12]</sup> Motivated by the potential for autonomous restoration of conductivity in damaged battery electrodes, here we investigate the encapsulation and release of carbon black suspensions.

The encapsulation of conductive nanoparticles is challenging due to the propensity to form a pickering emulsion that causes coalescence of particles in the capsule shell wall.<sup>[13]</sup> Also, the densities of the particles are generally higher than the suspension media, leading to settling of the particles. Caruso et al. successfully encapsulated pristine carbon nanotubes suspended in both chlorobenzene and ethyl phenylacetate, but the capsules were limited by significant nanotube agglomeration and low particle concentrations (0.5 mg/mL).<sup>[3]</sup> Stabilized suspensions of carbon nanotubes and graphene were later encapsulated by employing poly 3-hexylthiophene (P3HT) as a core additive, but particle concentrations remained limited to 0.5 mg/mL.<sup>[2]</sup> Jacobson et al. applied polymer coatings to the surface of titanium dioxide and black pigment particles to match the particle density to the suspension media.<sup>[14]</sup> Other methods to create stable particle suspensions include the use of surfactants to stabilize particles and hollow particles to lower the density.<sup>[15,16]</sup> Nonconductive polymer coatings and surfactant layers both

S. Kang, Prof. N. R. Sottos  
Beckman Institute for Advanced Science  
and Technology

Department of Materials Science and Engineering  
University of Illinois at Urbana-Champaign  
61801, USA  
E-mail: n-sottos@illinois.edu

A. R. Jones  
Beckman Institute for Advanced Science and Technology  
Department of Mechanical Engineering  
University of Illinois at Urbana-Champaign  
61801, USA

Prof. J. S. Moore  
Beckman Institute for Advanced Science and Technology  
Department of Chemistry  
University of Illinois at Urbana-Champaign  
61801, USA

Prof. S. R. White  
Beckman Institute for Advanced Science and Technology  
Department of Aerospace Engineering  
University of Illinois at Urbana-Champaign  
61801, USA

DOI: 10.1002/adfm.201303427



reduce the conductivity of the particle network and are therefore not desirable for conductive suspensions.

For conductivity restoration stable particle suspensions must be created to avoid entrapment of particles in the capsule shell wall or settling within the core without reducing particle conductivity. In addition, high particle loading and efficient particle release are desirable. Chen et al. prepared stable carbon nanotube solutions in common organic solvents by attaching octadecyl chains to the edge of nanotubes.<sup>[17]</sup> In this paper, we investigated two surface functionalization methods to attach hydrophobic octadecyl chains on carbon black surfaces with different surface densities. Stable carbon black suspensions were obtained in *o*-dichlorobenzene, enabling encapsulation. We studied the effects of carbon black particle concentrations and core thickeners on capsule stability, release of core content after crushing and potential for electrical conductivity restoration in battery electrodes.

## 2. Results and Discussion

### 2.1. Dispersion and Suspension of Carbon Black

The hydrophobicity of carbon black was tailored through surface functionalization to match that of the core solvent. Oxidized carbon black (OCB) was selected as the starting material because of its enriched surface reactive functional groups (e.g. carboxylic acid, carbonyl, phenolic hydroxyl, and lactone). Enhanced hydrophobicity was achieved through covalent

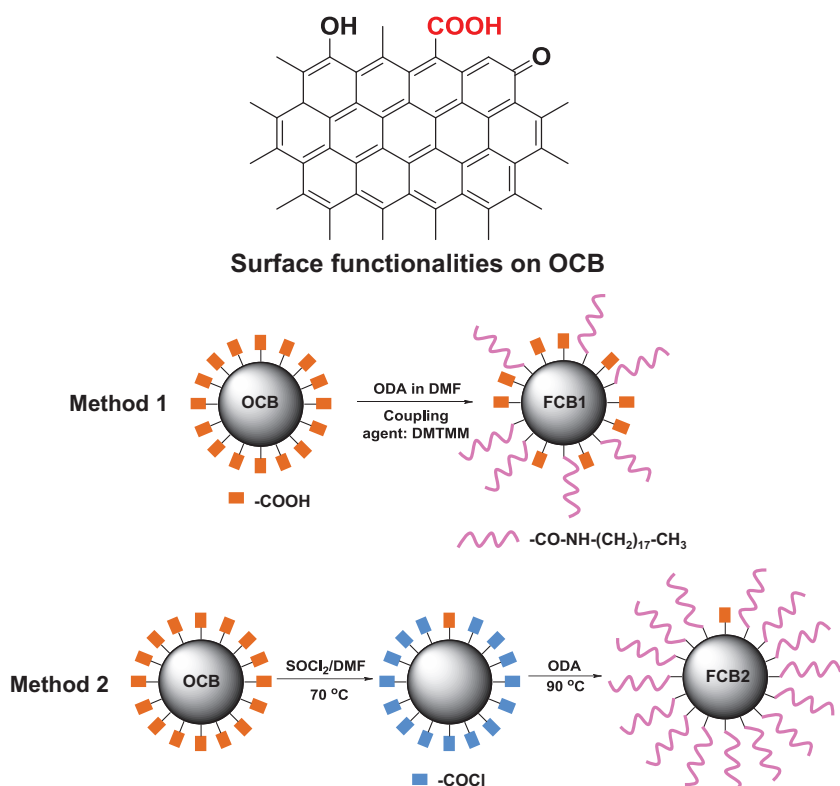
bonding of octadecyl ( $-C_{18}H_{37}$ ) groups on the OCB surface by two different methods (**Scheme 1**).

While the target products were the same, the conversion ratio varied depending on the method of functionalization. The amount of unconverted carboxylic acid groups on the carbon black surface was determined by titration. The carboxylic acid content in as-received OCB was 0.103 meq/g, as expected from prior literature.<sup>[18]</sup> FCB1 contained 0.055 meq/g and FCB2 contained 0.008 meq/g carboxylic acid, yielding a conversion ratio of 47% and 92%, respectively. The surface density of octadecyl groups on FCB2 was about twice that of FCB1, yielding an increased hydrophobicity of FCB2 relative to FCB1. The CHN elemental analysis results (Table S1) also showed increasing nitrogen content from FCB1 to FCB2 resulting from amide bond formation.

To evaluate the dispersion of FCBs, we measured the particle agglomerate sizes in several weakly polar solvents: *o*-dichlorobenzene (*o*-DCB), ethyl phenylacetate (EPA), hexyl acetate (HA), and dibutyl phthalate (DBP) using dynamic light scattering (DLS) (**Table 1**). Data for unfunctionalized OCB and acetylene carbon black (ACB) are also included in Table 1 for comparison. Unlike OCB, ACB is a type of conventional carbon black with fewer hydrophilic surface functional groups. Both OCB and ACB have single particle diameters of ca. 40 nm (Figure S1 in supporting information). In weakly polar solvents, the particle agglomerate sizes for both FCB1 and FCB2 were smaller than that of OCB and ACB, suggesting enhanced dispersions due to increased surface hydrophobicity. Wu et al.<sup>[19]</sup> have also reported that the bulky surface octadecyl groups minimize electrostatic interaction between carbon black particles and reduce agglomeration. The relatively larger FCB2 agglomerate size compared to FCB1 is likely due to the formation of ester bonds by the reactive acyl chloride groups on one carbon black particle with the hydroxyl groups of neighboring particles during the first step of preparing FCB2. The best dispersion was achieved in *o*-DCB, which was selected as the solvent for encapsulation.

Two types of core thickeners, Bisphenol A diglycidyl ether (DGEBA, trade name EPON 828) and poly 3-hexylthiophene (P3HT), were also examined by dissolving in *o*-DCB. The addition of the core thickeners did not significantly change the agglomerate sizes.

The long term stability of suspended carbon black particles in the core solvent is of particular importance, since the precipitation of carbon black after encapsulation can lead to reduced carbon black release upon capsule rupture. Re-agglomeration of ACB and OCB in *o*-DCB was observed after 2 h of DLS measurement while both FCB1 and FCB2 retained uniform dispersions (Figure S2). The particle concentrations of aliquots taken from the top layer of carbon black suspensions in scintillation vials were monitored by UV-visible spectroscopy,



**Scheme 1.** Surface functionalization of OCB. Octadecyl groups were covalently attached on the OCB surface by two methods, yielding different conversion ratios.

**Table 1.** Particle size distribution of different types of carbon black in various solvents.

solvent	Z-average particle size, diameter [nm]			
	OCB	ACB	FCB1	FCB2
o-DCB	725 ± 614	285 ± 201	156 ± 84	169 ± 97
HA	961 ± 868	3365 ± 2211	821 ± 522	897 ± 731
EPA	3835 ± 2119	3684 ± 2406	1357 ± 789	1862 ± 1168
DBP	1724 ± 1140	2446 ± 1478	265 ± 169	552 ± 401
o-DCB/DGEBA	500 ± 368	312 ± 229	112 ± 50	265 ± 158
o-DCB/P3HT	294 ± 216	961 ± 699	204 ± 103	143 ± 49

as shown in **Figure 1**. All types of carbon black precipitated within one day in EPA and HA. A slower precipitation rate was observed in DBP, primarily due to its high viscosity. In contrast, FCBs showed good suspension stability in o-DCB, with only a minimal concentration decrease over 20 days. FCB2 exhibited slightly better stability than FCB1 due to the higher octadecyl

surface coverage. A significantly lower concentration of OCB and ACB in o-DCB was observed.

## 2.2. Encapsulation of Carbon Black

Varying types and concentrations of carbon black were encapsulated in polyurethane (PU)/poly(urea-formaldehyde) (PUF) double shell wall microcapsules. Capsules with diameters ranging from 20–240 µm were produced by mechanical agitation (**Figure 2a**). Smaller capsules (less than 10 µm in diameter) were achieved by using a homogenizer (**Figure 2b**). A summary of all the different encapsulated core materials is provided in **Table 2**. The maximal particle loading achieved was 0.2 g/mL (~13% in volume), which represents a significant improvement compared to recently published values for carbon based particle encapsulations.<sup>[2,3,5–8,14]</sup> Further increase of the FCB loading led to high viscosity and immobility of the core. No residual carbon black was observed in the aqueous phase after encapsulation, indicating nearly complete encapsulation of FCB. In contrast,

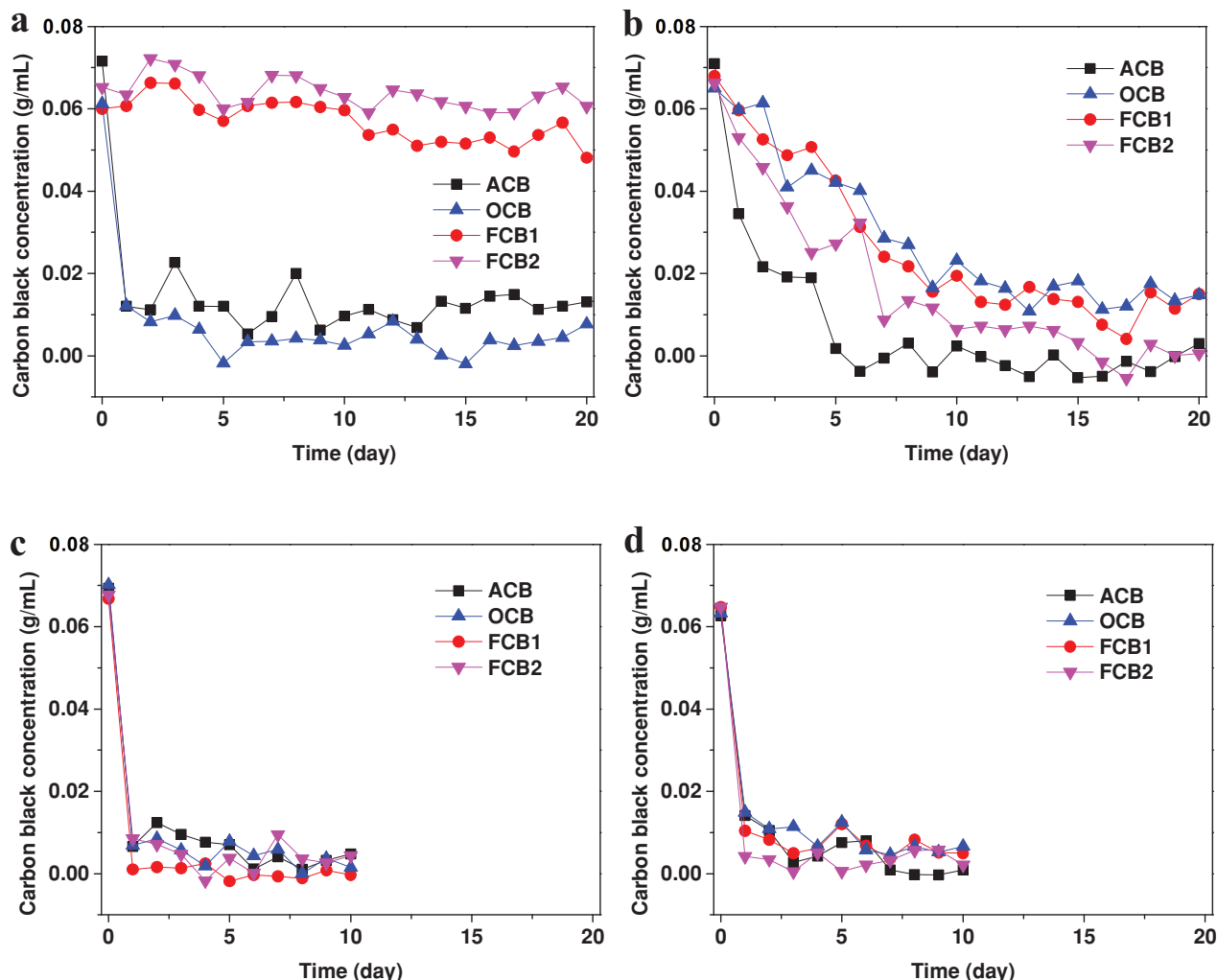


**Figure 1.** Concentration change of carbon black in suspensions (top layer) measured by UV-visible spectroscopy. The suspension solvents are a) o-DCB, b) DBP, c) EPA, and d) HA.

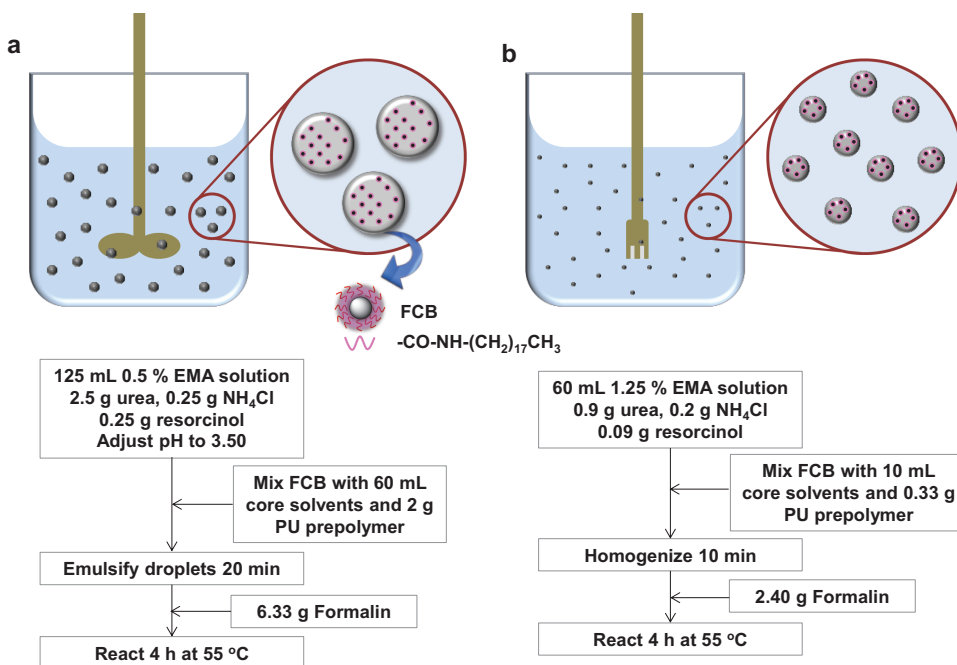


**Figure 2.** Encapsulation methods for preparing PU/PUF double shell wall microcapsules containing FCB in solvent using a) mechanical agitation and b) homogenization.

a maximum loading of only 0.05 g/mL (~3% in volume) ACB was encapsulated. OCB was not able to be encapsulated due to the migration of the hydrophilic particles from the core to the aqueous phase during encapsulation.

Scanning electron microscopy (SEM) was performed to characterize microcapsule morphology. As shown in Figure 3a,

**Table 2.** Summary of different encapsulated core materials.

Microcapsule type	Carbon black concentration [g/mL]	Core thickener concentration [g/mL]
NCB (no carbon black)	0	0
NCB/DGEBA	0	0.33 g/mL DGEBA
NCB/P3HT	0	0.01 g/mL P3HT
ACB	0.05 g/mL ACB	0
FCB1L	0.067 g/mL FCB1	0
FCB1L/DGEBA	0.067 g/mL FCB1	0.33 g/mL DGEBA
FCB1M/DGEBA	0.133 g/mL FCB1	0.33 g/mL DGEBA
FCB1H/DGEBA	0.200 g/mL FCB1	0.33 g/mL DGEBA
FCB1L/P3HT	0.067 g/mL FCB1	0.01 g/mL P3HT
FCB1L/P3HT (2 μm <sup>a)</sup>	0.067 g/mL FCB1	0.01 g/mL P3HT
FCB1M/P3HT	0.133 g/mL FCB1	0.01 g/mL P3HT
FCB1H/P3HT	0.200 g/mL FCB1	0.01 g/mL P3HT
FCB2L	0.067 g/mL FCB2	0
FCB2L/P3HT	0.067 g/mL FCB2	0.01 g/mL P3HT
FCB2M/P3HT	0.133 g/mL FCB2	0.01 g/mL P3HT
FCB2H/P3HT	0.200 g/mL FCB2	0.01 g/mL P3HT

<sup>a)</sup>Average microcapsule diameter is 2 μm. All the other types of capsules are ca. 100–300 μm in diameter.

the microcapsule exterior surface consists of a smooth and continuous PUF layer with embedded PUF nanoparticles.<sup>[20]</sup> The cross-sectional image of a ruptured capsule (Figure 3b, embedded in epoxy matrix) shows a ca. 200 nm thick microcapsule shell wall composed of PUF and a rough inner layer composed of PU and embedded carbon black particles entrapped by the PU prepolymer during encapsulation. The smaller microcapsules (Figure 3c,d) with 2 μm average diameter prepared by the homogenization method had a smoother exterior surface and thinner shell wall of ca. 40 nm.

Microcapsule size decreased with increasing agitation rate following a power law relationship (Figure 4a).<sup>[21]</sup> A broader size distribution was observed for all FCB1 filled microcapsules (Figure 4b,c) as compared to solvent-only systems.<sup>[22,23]</sup> We hypothesized that the high viscosity of the continuous organic phase caused the coalescence of small emulsion droplets during encapsulation and broadened the size distribution. The microcapsule size increased from 133 μm to 259 μm after tripling the FCB1 loading from 0.067 g/mL to 0.2 g/mL (in the presence of 0.33 g/mL DGEBA, 400 rpm agitation rate) due to the increase of core viscosity.

The addition of core thickeners (DGEBA and P3HT) into the encapsulated core led to an increase of core viscosity, as shown in Table 3. The mixture viscosity was doubled by increasing the concentration of core thickeners in o-DCB. A lower concentration of P3HT than DGEBA was required to reach the same viscosity of the mixture. This difference is primarily due to the extended long chain conformation of P3HT in o-DCB, which is absent in DGEBA.

Thermal stability of microcapsules was characterized by thermal gravimetric analysis (TGA). Representative TGA curves of different microcapsules are shown in Figure 5a. Distinct weight loss was observed for all microcapsules with an onset

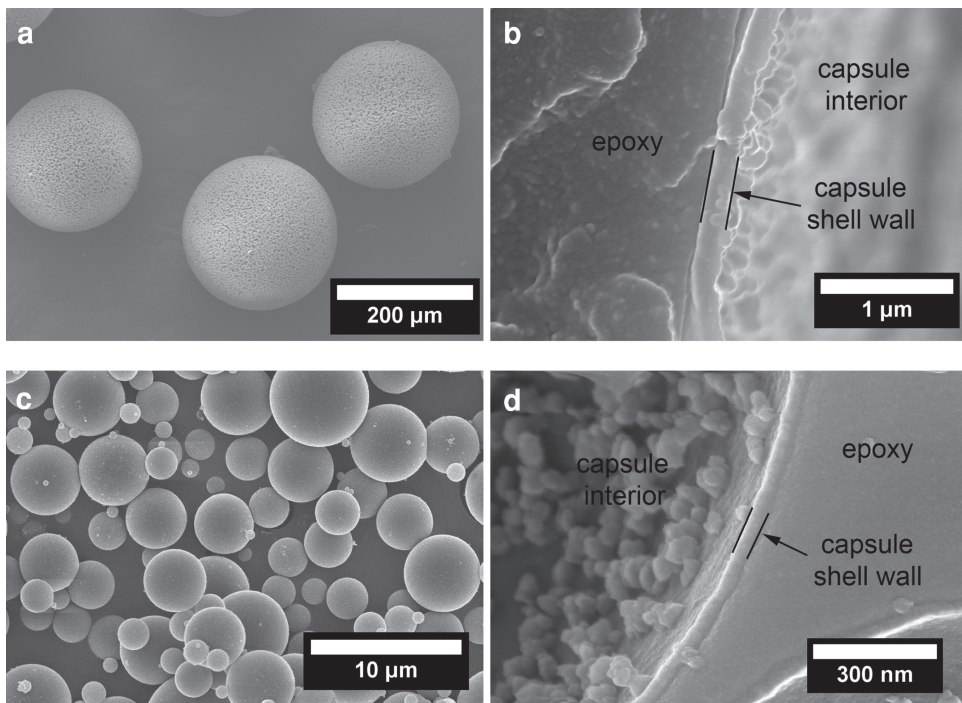


**Figure 3.** SEM images of FCB1H/P3HT microcapsules. a) Large microcapsules (100–300  $\mu\text{m}$  average diameter) have a rough exterior surface. b) Cross section of large microcapsules reveals microcapsule shell wall of ca. 200 nm. c) Small microcapsules (2  $\mu\text{m}$  average diameter) have a smooth exterior surface. d) Cross section of small microcapsules reveals microcapsule shell wall of ca. 40 nm.

temperature of 160 °C attributed to the start of o-DCB (bp 180 °C) evaporation. For the microcapsules containing DGEBA (0.33 g/mL), the mass loss from 265 to 445 °C was attributed to decomposition of the resin component. The decomposition of P3HT was not detected due to its low concentration (0.01 g/mL). An isothermal study of microcapsules was conducted at 60 °C or 150 °C for 2 h (Figure 5b,c). The weight loss of all microcapsules was less than 0.7 wt% at 60 °C and less than 2 wt% at 150 °C. Based on thermal stability, the incorporation of FCB and core thickeners did not compromise the capsule shell wall quality.

### 2.3. Release of Carbon Black Upon Capsule Rupture

The release of carbon black particles was examined by optical microscopy and SEM after microcapsules were ruptured by crushing between two glass slides. As shown in Figure 6a–c, ACB filled microcapsules had no visible particle release. In aliquots of the encapsulation emulsion taken prior to microcapsule shell wall formation, ACB particles preferentially resided on the oil/water interface and showed no movement due to the adsorption of surfactant. As a result, ACB particles were entrapped in the shell wall during encapsulation. In contrast, the FCB1 and FCB2 microcapsules both exhibited particle release, especially FCB2 (Figure 6d–i). Fast brownian motion of the FCB particles in the oil phase was observed in the emulsion prior to encapsulation, suggesting a minimal effect from surfactant adsorption. Adsorption by PU prepolymer and adhesion

to the capsule shell wall inhibited the release of FCB1. The enhanced particle release of FCB2 is due to the higher octadecyl group coverage of FCB2 compared to FCB1.

The addition of core thickeners, DGEBA and P3HT, further promoted the release of FCB particles. In the absence of core thickener, FCB1 capsules showed a small amount of particle release upon rupture (Figure 6d–f). A clear trend of enhanced FCB1 release by incorporating DGEBA and P3HT into the core was observed in Figure 6j–l and m–o. By dispersing FCB in a more viscous core, adsorption by PU prepolymer was minimized and adhesion to capsule shell wall was reduced. Furthermore, P3HT has the ability to stabilize dispersed FCB suspensions through  $\pi$ - $\pi$  stacking interactions.<sup>[24]</sup> The combined viscosity enhancement and aromatic stacking effects make P3HT a superior candidate as a core thickener for stabilizing FCB suspensions.

### 2.4. Anode Conductivity Restoration

The restoration of conductance in a battery anode material was evaluated by a fiber removal protocol (Figure S3) in which a line crack (ca. 10  $\mu\text{m}$  width) was created on a nanoparticle Si anode by removing a glass fiber (8  $\mu\text{m}$  diameter) from underneath. Conductance restoration of the damaged Si anode was evaluated by either depositing the capsule core material (~1 mg) directly onto the crack region or crushing carbon black filled microcapsules (~1 mg) on the line crack. Figure 7 shows the line crack in the anode prior to testing and

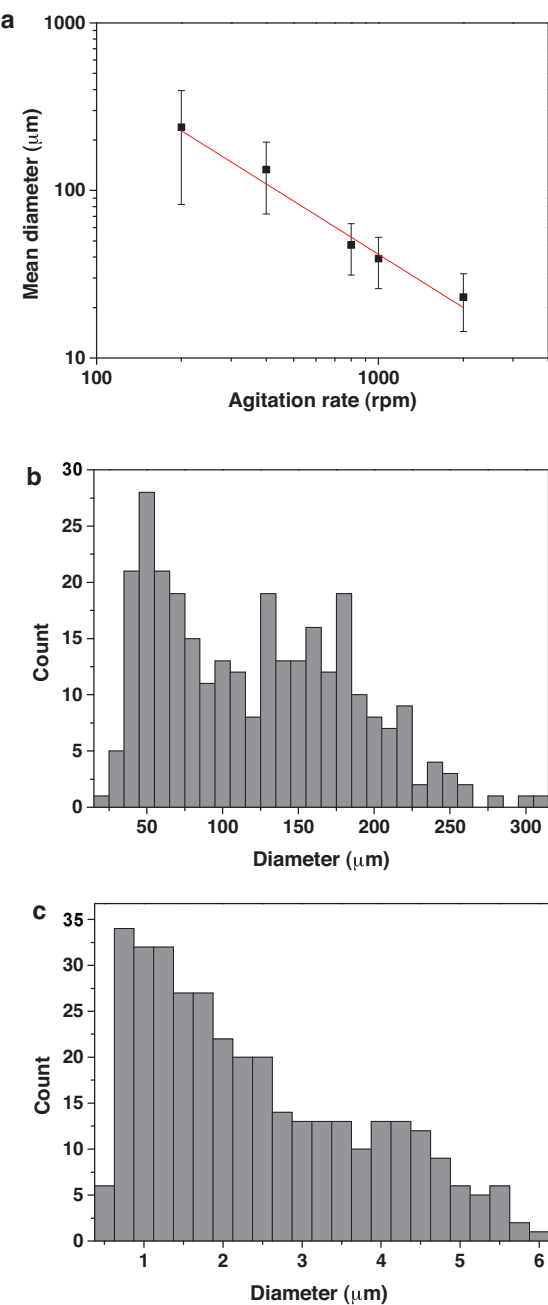


**Figure 4.** Size characterization of FCB1 filled microcapsules. a) Mean diameter of FCB1L/DGEBA microcapsules obtained by optical measurement as a function of agitation rate. Vertical error bars represent one standard deviation. b) Representative microcapsule diameter histogram showing the size distribution for capsules made by mechanical agitation at 400 rpm (Average diameter = 133  $\mu\text{m}$ ). c) Representative microcapsule diameter histogram showing the size distribution for capsules made by homogenization (Average diameter = 2  $\mu\text{m}$ ).

**Table 3.** Viscosity of *o*-DCB/core thickener mixtures.

Mixture	<i>o</i> -DCB	0.17 g/mL DGEBA in <i>o</i> -DCB	0.33 g/mL DGEBA in <i>o</i> -DCB	0.01 g/mL P3HT in <i>o</i> -DCB	0.02 g/mL P3HT in <i>o</i> -DCB
Viscosity [cP]	1.31	2.20	4.44	2.60	5.04

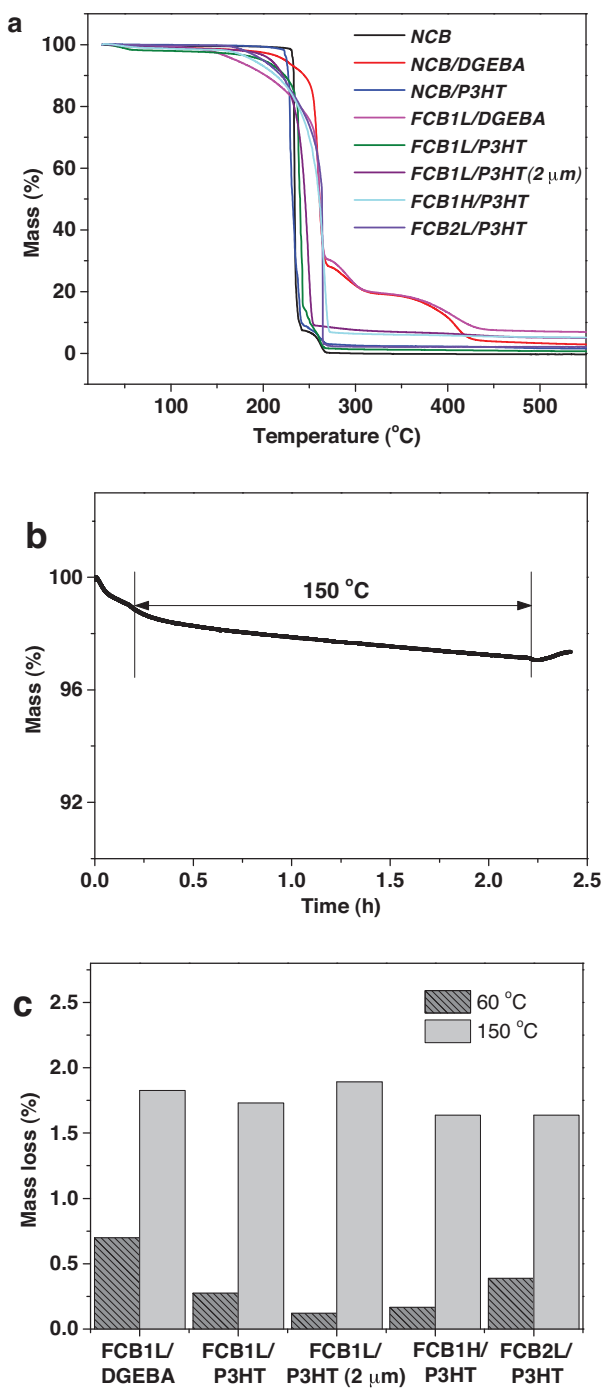


**Figure 5.** Thermal characterization of microcapsules. a) Dynamic TGA curves of prepared microcapsules with varying core contents. Encapsulated core materials are defined in Table 2. b) Representative iso-thermal curve of FCB1L/P3HT microcapsules at 150 °C. c) Percentage mass loss of microcapsules under isothermal condition (60 °C and 150 °C, 2 h).

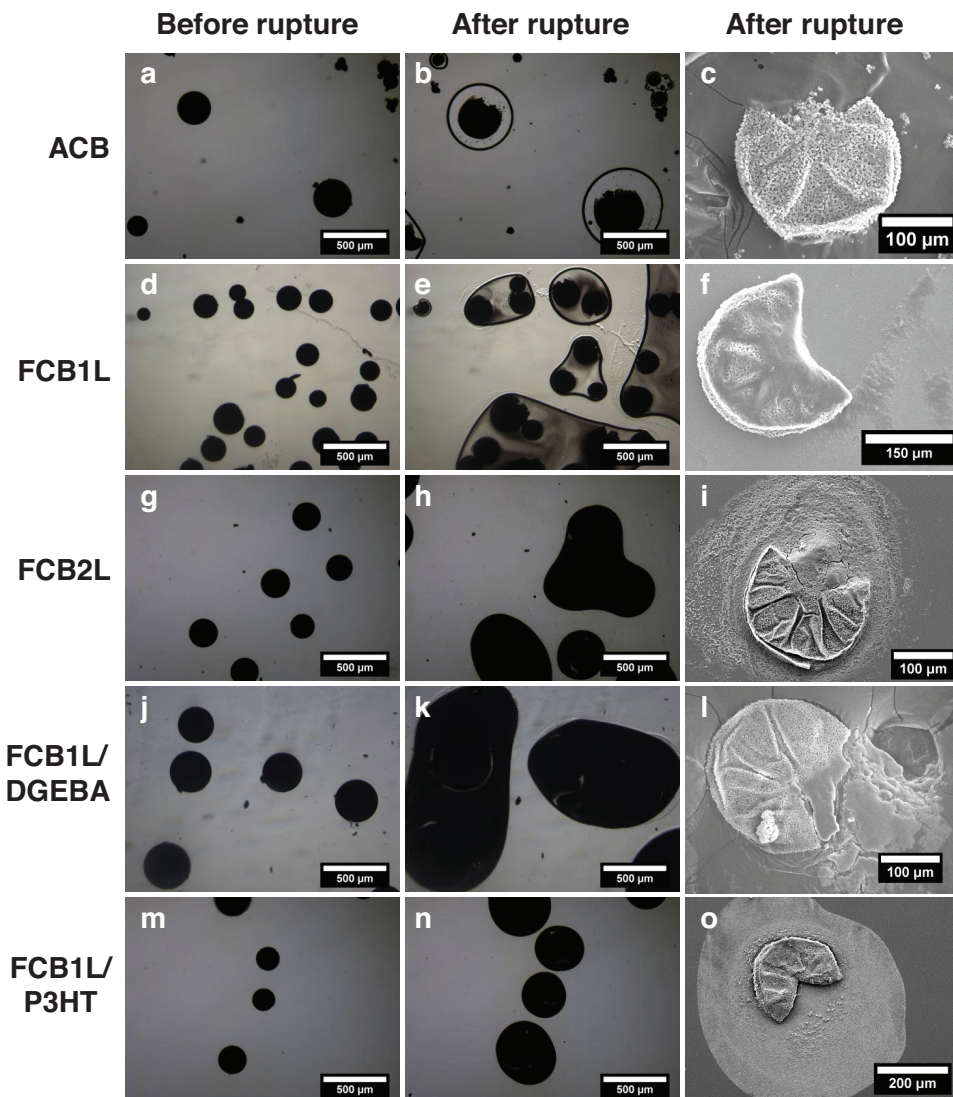


**Figure 6.** Optical and SEM images of pristine and ruptured carbon black microcapsules with different cores. Column 1 and Column 2 contain optical images of microcapsules before and after rupture, respectively. Column 3 contains SEM images of ruptured microcapsules and the released core. a–c) ACB, d–f) FCB1L, g–i) FCB2L, j–l) FCB1L/DGEBA, m–o) FCB1L/P3HT. Capsule core contents are summarized in Table 2.

the release of FCB1 particles on the line crack after capsule crushing. Removal of the fiber resulted in complete loss of conductivity across the anode. Direct deposition of the core material (Figure S4a) led to a monotonic increase of conductance with time as the solvent evaporated. Full recovery was obtained after ca. 400 s. When microcapsules were crushed directly on the line crack, full recovery was reached after about 500 s (Figure S4b).

The conductance restoration efficiency is defined as:

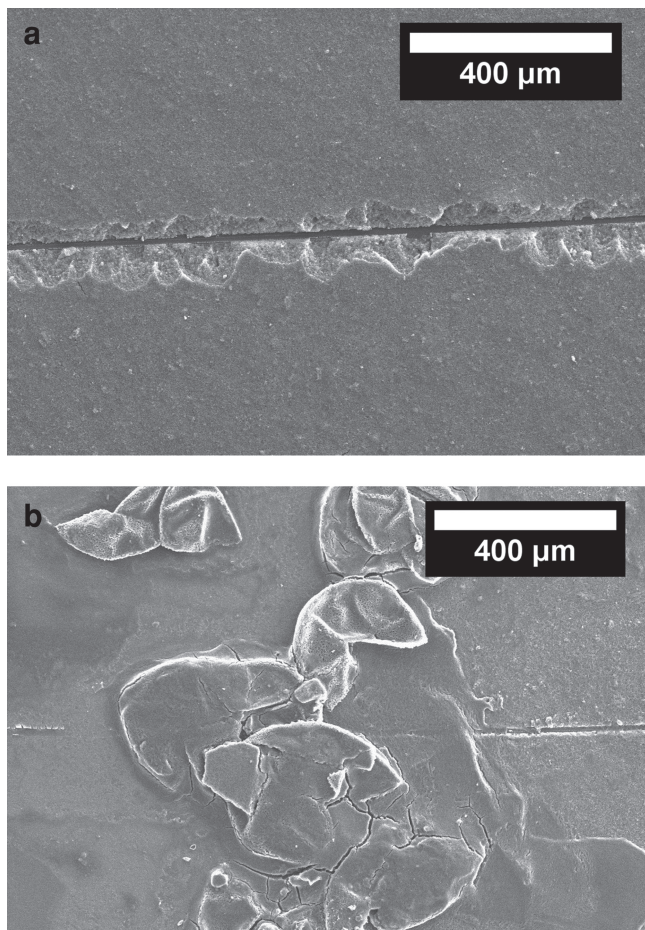
$$\eta_G = \frac{G_h}{G_0} \quad (1)$$

where  $G_h$  is the anode conductance after healing, and  $G_0$  is the initial anode conductance. The initial conductance of the Si anodes varied from 1.4 to  $2.0 \times 10^{-5} \Omega^{-1}$ . Microcapsules with different core materials and different sizes were tested

and the conductance restoration results are presented in Figure 8.

For the microcapsules containing FCB1 and 0.33 g/mL DGEBA (Figure 8a), we obtained a maximum restoration efficiency of  $77 \pm 12\%$ . The FCB1 loading and capsule size greatly influenced the restoration efficiency. Higher FCB1 loading and larger capsule diameters led to higher conductance restoration efficiency due to increased delivery of carbon black to the damaged region. The direct deposition of core solution on line cracks yielded 100% conductance restoration for all three FCB1 loadings. In contrast, control experiments with solvent only microcapsules produced no healing due to the absence of conductive particles.

When P3HT was used as core thickener instead of DGEBA in FCB1 microcapsules, the conductance restoration efficiency increased to greater than 85% for all tests (Figure 8b and



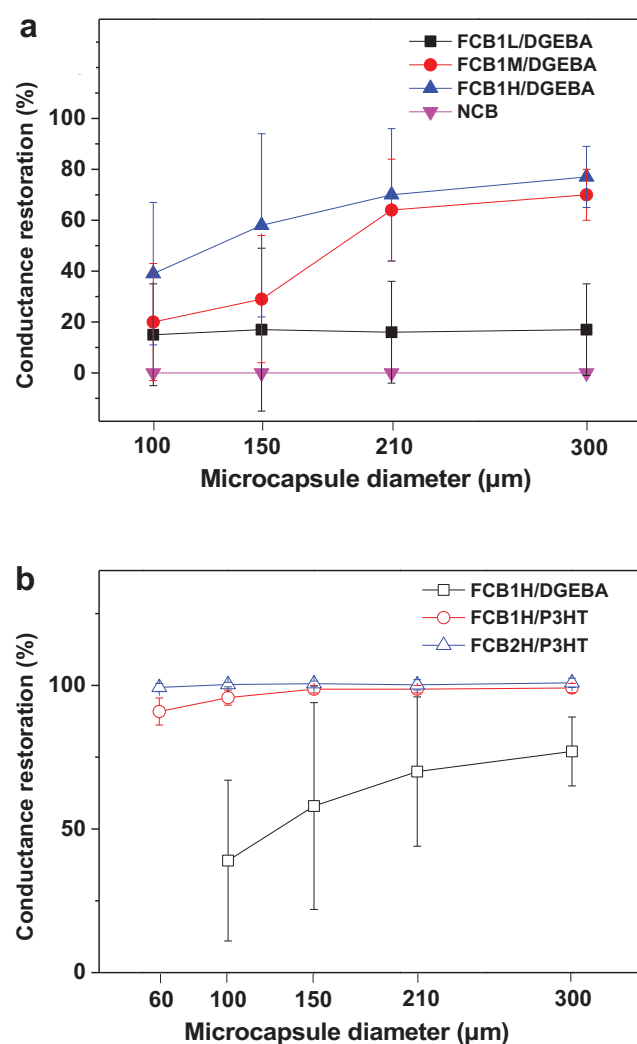
**Figure 7.** SEM images of a) a line crack introduced by fiber removal protocol in a nanoparticle Si anode and b) ruptured FCB1H/DGEBA micro-capsules and release of carbon black onto a line crack.

Figure S5a). Full conductance recovery was achieved in micro-capsules with 0.2 g/mL FCB1 for capsule diameters of 150 μm and above. The improved performance is attributed to the lower concentration of P3HT (0.01 g/mL) compared to DGEBA (0.33 g/mL) in the core solution and the higher concentration of FCB1 particles for capsules with P3HT. The restoration efficiency for P3HT capsules also showed less dependence on capsule size. The capsules containing commercial P3HT showed similar conductance restoration efficiency for all the given sizes.

The highest level of conductance restoration was achieved with FCB2 micro-capsules containing P3HT core thickener (Figure 8b and Figure S5b). Restoration efficiencies in the range of 95–100% were achieved for all capsule diameters. The high octadecyl surface coverage for FCB2 facilitates better release upon capsule rupture (Figure 8g–i), delivering more particles to the site of damage and leading to full recovery of anode conductance.

### 3. Conclusion

Two types of FCB with different hydrophobicity were prepared by controlling the concentration of octadecyl chains on the



**Figure 8.** Conductance restoration of nanoparticle Si anodes comparing a) various FCB1 and b) FCB1 and FCB2 filled micro-capsules with different diameters and carbon black loadings.

particle surface. Surface functionalization resulted in improved dispersion properties and suspension stability of carbon black in *o*-DCB due to an increased hydrophobicity from octadecyl groups. Robust micro-capsules with high loading of FCB (up to 0.2 g/mL) were achieved. The capsule size was controlled from submicron to a few hundred microns. The capsules also exhibited good stability at elevated temperature (150 °C). Substantial particle release was observed after crushing of FCB micro-capsules. The incorporation of DGEBA or P3HT as core thickener increased the amount of FCB release by increasing the core viscosity and stabilizing the particles. Release of FCB particles from micro-capsules resulted in conductance restoration of a damaged silicon anode. The concentration of core thickeners and the hydrophobicity of the FCB greatly influenced the conductance restoration efficiency. A full recovery of anode conductance was achieved with micro-capsules containing P3HT and hydrophobic FCB.

## 4. Experimental Section

**Materials:** ACB (100% compressed) was purchased from Alfa Aesar. OCB with the commercial name Regal® 400 was obtained from Cabot Corporation. Dimethyl formamide (DMF), ethyl acetate, toluene, o-dichlorobenzene (o-DCB), ethyl phenylacetate (EPA), hexyl acetate (HA), dibutyl phthalate (DBP), 4-(4,6-dimethoxy-1,3,5-triazin-2-yl)-4-methylmorpholinium chloride (DMTMM), octadecylamine (ODA), 3-hexyl thiophene, ferric chloride, chloroform, ammonia, ethylenediaminetetraacetic acid (EDTA), urea, formalin solution (37 w/v%), ammonium chloride, resorcinol, and sodium bicarbonate were used as received from Sigma Aldrich. The commercial polyurethane (PU) prepolymer, Desmodur L 75, was generously provided by Bayer Material Science and used as received. Desmodur L 75 is a prepolymer solution in ethyl acetate with a reported equivalent weight of 315 g and an isocyanate content of  $13.3 \pm 0.4$  wt%. Ethylene-maleic anhydride (EMA) copolymer (Zemac-400) powder ( $M_w \sim 400$  kDa) was obtained from Vertellus and used as a 2.5 wt% aqueous solution. Diglycidyl ether of bisphenol A resin (DGEBA, trade name EPON 828) was used as received from Miller-Stephenson.

**Functionalization of Carbon Black Particles:** Two approaches were used to prepare FCB, as described in Scheme 1. In method 1,<sup>[25]</sup> a stock suspension of OCB in DMF (2.5 w/v%, 160 mL) was prepared and sonicated for 12 h prior to use. The functionalization was carried out by adding DMTMM (0.24 g) and ODA (0.24 g) into the carbon black suspension and reacting for 120 h while stirring. FCB1 was separated by centrifugation and subsequently rinsed with ethyl acetate ( $5 \times 120$  mL) to remove residual DMTMM and ODA. In method 2,<sup>[17]</sup> OCB (2 g) was stirred in  $\text{SOCl}_2$  (60 mL) and DMF (4 mL) at  $75^\circ\text{C}$  for 24 h. The product was separated by centrifugation and then washed with anhydrous toluene. After complete removal of solvent by vacuum drying, the solid was mixed with ODA (4 g) and heated at  $90^\circ\text{C}$  for 96 h. The ODA was removed by rinsing the crude product with ethyl acetate ( $5 \times 60$  mL) with 20 min of sonication for each rinsing step.

**Characterization of FCB:** The average sizes of carbon black agglomerates in different solvents were measured by DLS using a Zetasizer Nano ZS (Malvern Instruments Ltd). Suspensions with 2.5 mg/g particle concentration were sonicated 3 min prior to measurement. In order to quantify the conversion ratio of carboxylic acid groups after functionalization, the -COOH content of the different types of carbon black was measured by titrating with  $\text{NaHCO}_3$  solution.<sup>[26]</sup> The finishing point of titration was at the maximum consumption of  $\text{NaHCO}_3$  for neutralization.

The stability of carbon black suspensions in different solvents was studied by UV-visible spectroscopy (UV-2401 PC, Shimadzu, Japan). Based on the Lambert-Beer law, a linear calibration curve of carbon black concentration as a function of absorbance (@ 800 nm) was created by measuring the absorbance of carbon black suspensions (400 to 900 nm) with five known concentrations. For the stability study, a carbon black suspension was prepared (0.067 g/mL) and allowed to settle without perturbation. An aliquot of the top layer suspension was taken and diluted 1000 times with the corresponding organic solvent at certain time intervals. The absorbance was then measured by UV-vis and the carbon black concentration was determined from the calibration curve.

**Synthesis of P3HT:** P3HT was prepared by the oxidative coupling polymerization of 3-hexyl thiophene according to the procedure described by Sugimoto.<sup>[27]</sup> Ferric chloride (7.8 g, 0.048 mol) was stirred in chloroform (95 mL). 3-hexylthiophene (2 g, 0.012 mol) was instantly added into the suspension. After 20 min, the reaction was terminated by the addition of deionized water. The solid product was precipitated from acidic ethanol. Subsequently, the crude product was redissolved in chloroform and the insoluble part was removed by filtering. The clear orange solution was washed by ammonia ( $3 \times 60$  mL), EDTA solution ( $3 \times 60$  mL), and water ( $3 \times 60$  mL) successively. The final product was obtained by precipitation in ethanol, filtering, and drying. GPC (eluent: tetrahydrofuran):  $M_n$ : 44251,  $M_w/M_n$ : 2.20.  $^1\text{H}$  NMR (500 MHz,  $\text{CDCl}_3$ ,  $\delta$ ): 6.98 (br m, 1 H), 2.80 and 2.56 (br m, 2 H), 1.80–1.10 (br m, 8

H), 0.91 (br m, 3 H). Degree of regioregularity (ratio of head-to-tail configuration): 79%.

**Preparation of Carbon Black Suspension Filled Microcapsules:** The encapsulation procedure (Figure 3a) was adapted from an established PU/PUF double shell wall method.<sup>[21]</sup> The carbon black particles were dispersed in a core solvent mixture (o-DCB with appropriate amount of DGEBA or P3HT) with the assistance of sonication (tapered 1/800 tip sonication horn of a 750-W ultrasonic homogenizer, Cole Parmer) for at least 2 min. PU prepolymer (0.033 g/mL) was subsequently added to the encapsulation core. Upon the dissolution of PU prepolymer, the encapsulation core was added into the aqueous media at a specific stirring rate. The capsules contained 0.33 g/mL DGEBA or 0.01 g/mL P3HT in o-DCB. The microcapsules were rinsed with water to remove residual EMA surfactant and then filter dried to obtain free-flowing microcapsules.

Microcapsules with diameter less than 10  $\mu\text{m}$  were produced by a homogenization (OMNI GLH-01) method (Figure 3b). Homogenization was effective in reducing the emulsion droplets to submicron size as compared to mechanical agitation method. The microcapsules were centrifuged and washed with water three times to remove the residual surfactant, and then freeze dried to obtain a free-flowing powder.

**Characterization of Microcapsules:** Microcapsule morphology was investigated by SEM (Hitachi 4800). Before imaging, samples were sputter-coated with Au/Pd to eliminate charging effects. For capsule shell wall characterization, fully cured epoxy (DGEBA/12 pph DETA) samples containing 5 wt% microcapsules were fractured to expose the ruptured microcapsule shell wall. The fractured pieces were then sonicated to remove encapsulated materials and leave only the capsule shell wall for imaging.

Microcapsule size distributions were obtained by analyzing the optical images of microcapsules (imaged by Leica DMR Optical Microscope) prepared at different agitation rates. For microcapsules with diameter less than 10  $\mu\text{m}$ , size distributions were determined from analyzing SEM images. ImageJ software was used to measure microcapsule diameter and obtain statistical data.

TGA was performed on a Mettler-Toledo TGA851, calibrated by indium, aluminum, and zinc standards with a heating rate of  $10^\circ\text{C}/\text{min}$  from 25 to  $600^\circ\text{C}$  under nitrogen atmosphere. Isothermal studies of capsules were performed at  $60^\circ\text{C}$  and  $150^\circ\text{C}$  for 2 h, respectively. Viscosity of encapsulated core solvents was measured with a TA Instrument AR-G2 rheometer using the double-wall concentric cylinders geometry.

**Conductivity Restoration of Fractured Si Anodes:** Silicon anode specimens for evaluating conductance restoration were fabricated with a controlled crack size by a fiber removal method (Figure S3). An 8  $\mu\text{m}$  diameter glass fiber was adhered to a glass slide by tape. The glass slide was then dipped in titanium butoxide solution (9%) in ethanol and dried. The Ti (IV) butoxide served as a blocking layer to prevent the penetration of Si anode slurry into the gap between the glass fiber and the glass slide. The Si anode slurry consisted of 7 wt% Si nanoparticles (100 nm), 2 wt% carboxymethyl cellulose (CMC), and 1 wt% ACB in deionized water. A doctor blade was used to cast a uniform layer of the slurry on glass. After drying at room temperature for 24 h, the fiber was carefully pulled out, creating a 10  $\mu\text{m}$  wide line crack on the Si anode. FCB filled microcapsules were deposited onto the line crack and crushed with a cover slide. The conductance change of the Si anode was measured by a Wheatstone bridge setup described previously by Blaiszik et al.<sup>[1]</sup> The specimen conductance  $G$  was calculated,

$$G = \frac{G_B}{\frac{V_B}{V_G} + \frac{G_1}{G_1 + G_2}} \quad (2)$$

where  $V_B$  is the bridge voltage,  $V_G$  is supplied voltage ( $V_G = 5$  V), and  $G_1$ ,  $G_2$ , and  $G_3$  are the conductance of the other resistors ( $G_1 = 0.0909 \Omega^{-1}$ ,  $G_2 = 0.0091 \Omega^{-1}$ ,  $G_3 = 10^{-4} \Omega^{-1}$ ) in Wheatstone bridge, respectively.

## Supporting Information

Supporting Information is available from the Wiley Online Library or from the author.

## Acknowledgements

This work was supported as part of the Center for Electrical Energy Storage – Tailored Interfaces, an Energy Frontier Research Center funded by the U.S. Department of Energy, Office of Science, Office of Basic Energy Sciences under Award Number (919 DOE ANL 9F-31921NS). The authors would also like to thank Brett Krull for the viscosity measurement and Chunjie Zhang and Benjamin Blaiszik for helpful discussions.

Received: October 4, 2013

Revised: December 2, 2013

Published online: February 1, 2014

- [1] B. J. Blaiszik, S. L. B. Kramer, M. E. Grady, D. A. McIlroy, J. S. Moore, N. R. Sottos, S. R. White, *Adv. Mater.* **2012**, *24*, 398.
- [2] S. A. Odom, T. P. Tyler, M. M. Caruso, J. A. Ritchey, M. V. Schulmerich, S. J. Robinson, R. Bhargava, N. R. Sottos, S. R. White, M. C. Hersam, J. S. Moore, *Appl. Phys. Lett.* **2012**, *101*, 043106.
- [3] M. M. Caruso, S. R. Schelkopf, A. C. Jackson, A. M. Landry, P. V. Braun, J. S. Moore, *J. Mater. Chem.* **2009**, *19*, 6093.
- [4] S. A. Odom, M. M. Caruso, A. D. Finke, A. M. Prokup, J. A. Ritchey, J. H. Leonard, S. R. White, N. R. Sottos, J. S. Moore, *Adv. Funct. Mater.* **2010**, *20*, 1721.
- [5] S. J. Pastine, D. Okawa, A. Zettl, J. M. J. Fréchet, *J. Am. Chem. Soc.* **2009**, *131*, 13586.
- [6] L. Sánchez-Silva, N. Gutiérrez, P. Sánchez, A. Romero, J. L. Valverde, *Chem. Eng. J.* **2012**, *181–182*, 813.
- [7] L. Sánchez-Silva, N. Gutiérrez, A. Romero, P. Sánchez, J. L. Valverde, *J. Anal. Appl. Pyrol.* **2012**, *94*, 246.
- [8] L. Reiters, *Exp. Mech.* **1977**, *17*, 188.
- [9] A. G. Tennyson, B. Norris, C. W. Bielawski, *Macromolecules* **2010**, *43*, 6923.
- [10] K. A. Williams, A. J. Boydston, C. W. Bielawski, *J. Roy. Soc. Interface* **2007**, *4*, 359.
- [11] N. Ding, J. Xu, Y. Yao, G. Wegner, I. Lieberwirth, C. Chen, *J. Power Sources* **2009**, *192*, 644.
- [12] H. Wu, Y. Cui, *Nano Today* **2012**, *7*, 414.
- [13] D. J. Voorn, W. Ming, A. M. van Herk, *Macromolecules* **2006**, *39*, 2137.
- [14] B. Comiskey, J. D. Albert, H. Yoshizawa, J. Jacobson, *Nature* **1998**, *394*, 253.
- [15] X. Li, Y. Xiong, L. Zou, M. Wang, Y. Xie, *Micropor. Mesopor. Mat.* **2008**, *112*, 641.
- [16] J. D. Albert, G. Crossley, K. Geramita, K. R. Amundson, M. L. Steiner, P. Przaic, A. Loxley, B. Comiskey, P. J. Valianatos, U.S. Patent 6839158, **1999**.
- [17] J. Chen, M. A. Hamon, H. Hu, Y. Chen, A. M. Rao, P. C. Eklund, R. C. Haddon, *Science* **1998**, *282*, 95.
- [18] J. M. O'Reilly, R. A. Mosher, *Carbon* **1983**, *21*, 47.
- [19] G. Wu, P. P. Yin, R. Y. Dai, M. Wang, H. Z. Chen, H. C. Li, D. Y. Liu, *J. Mater. Res.* **2012**, *27*, 653.
- [20] E. N. Brown, M. R. Kessler, N. R. Sottos, S. R. White, *J. Microencapsul.* **2003**, *20*, 719.
- [21] M. M. Caruso, B. J. Blaiszik, H. Jin, S. R. Schelkopf, D. S. Stradley, N. R. Sottos, S. R. White, J. S. Moore, *ACS Appl. Mater. Inter.* **2010**, *2*, 1195.
- [22] D. A. McIlroy, B. J. Blaiszik, M. M. Caruso, S. R. White, J. S. Moore, N. R. Sottos, *Macromolecules* **2010**, *43*, 1855.
- [23] B. J. Blaiszik, M. M. Caruso, D. A. McIlroy, J. S. Moore, S. R. White, N. R. Sottos, *Polymer* **2009**, *50*, 990.
- [24] J. Zou, L. Liu, H. Chen, S. I. Khondaker, R. D. McCullough, Q. Huo, L. Zhai, *Adv. Mater.* **2008**, *20*, 2055.
- [25] G. Blotny, *Tetrahedron* **2006**, *62*, 9507.
- [26] H. P. Boehm, E. Diehl, W. Heck, R. Sappok, *Angew. Chem. Int. Edit.* **1964**, *3*, 669.
- [27] R. Sugimoto, S. Takeda, H. B. Gu, K. Yoshino, *Chem. Express* **1986**, *1*, 635.